arXiv:2111.10039v1 [eess.SY] 19 Nov 2021

# Modeling Flash Memory Channels Using Conditional Generative Nets

**Simeng Zheng**, **Chih-Hui Ho**, and **Paul H. Siegel**
Electrical and Computer Engineering Dept., University of California, San Diego, La Jolla, CA 92093 U.S.A
{*sizheng,chh279,psiegel*}@*ucsd.edu*

***Abstract*—Understanding the NAND flash memory channel has become more and more challenging due to the continually increasing density and the complex distortions arising from the write and read mechanisms. In this work, we propose a data-driven generative modeling method to characterize the flash memory channel. The learned model can reconstruct the read voltage from an individual memory cell based on the program levels of the cell and its surrounding array of cells. Experimental results show that the statistical distribution of the reconstructed read voltages accurately reflects the measured distribution on a commercial flash memory chip, both qualitatively and as quantified by the total variation distance. Moreover, we observe that the learned model can capture precise inter-cell interference (ICI) effects, as verified by comparison of the error probabilities of specific patterns in wordlines and bitlines.**

***Index Terms*—Machine learning, Communication channel, Generative modeling, Flash memory.**

## I. Introduction

Realistic models for digital communication and storage channels are essential tools in the design and optimization of signal processing, detection, and coding algorithms that achieve peak performance. For NAND flash memories, the steady reduction in technology feature size and the increase in cell bit-density has been accompanied by diminished memory reliability. Sources of errors are manifold, including programming errors, inter-cell interference (ICI), cell wear during program/erase (PE) cycling, cell charge loss due to data retention, and read disturb effects. Consequently, there is a critical need for detailed models that can accurately characterize the complex behavior of threshold voltages and hard errors to facilitate the development of improved read channels and error correction capabilities.

Several models of threshold voltage distributions and hard error distributions supported by empirical measurements in NAND flash memories have appeared in the literature. For example, Parnell et al. [11] fitted a parametrized Normal-Laplace mixture model to experimental measurements of 2-bit per cell MLC NAND flash memory threshold voltage distributions, providing accurate results for program-erase cycling up to 10 times the nominal device lifetime. Luo et al. [9] proposed another model for MLC flash, based on a modified version of the Student's t-distribution and the power law, that was shown empirically to provide accurate predictions of threshold voltage distribution shifts due to increased wear from cycling. Taranalli et al. [16], [17] used a modified beta-binomial distribution to model the overdispersion phenomenon observed in empirical measurements of hard errors in 1X-nm and 2Y-nm MLC NAND flash devices. Performance simulation

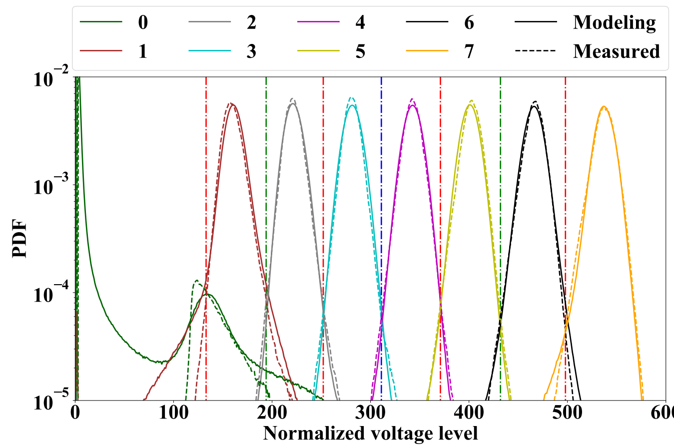


Fig. 1: The estimated probability density functions (PDFs) of measured data (dotted curves) and generative modeling data (solid curves) at 4000 program/erase (PE) cycles. The vertical dash-dotted lines are hard read thresholds.

results for a variety of error-correcting codes (ECC) confirmed that the model provided more accurate error-rate estimates than alternative models by accounting for the overdispersed error characteristics. As effective as these models have been in the scenarios to which they have been applied, they can not provide an accurate model of the complex spatio-temporal characteristics of flash memory read voltages.

Recently, there has been great interest in the application of machine learning in communications and networking, including data storage. For example, robust signal detection in magnetic recording channels using a recurrent neural network architecture was demonstrated in [18]. Recently, machine learning was also applied to page failure prediction [7], [15] and read voltage generation [8] in NAND flash memory. In view of the power of neural networks in learning highly complex multidimensional distributions, in this paper we propose the use of conditional generative nets as an approach to modeling flash memory read voltages in space and time.

The most popular generative model architectures currently are the generative adversarial network (GAN) [1] and the variational auto-encoder (VAE) [5]. Inspired by its promising results in two-dimensional (2-D) image reconstruction [4], we exploit the conditional VAE-GAN (cVAE-GAN) architecture to regenerate soft read voltages from program levels, using a dataset of measurements of a 1X-nm, 3-bit per cell TLC NAND flash memory.

We propose a novel generative modeling workflow to

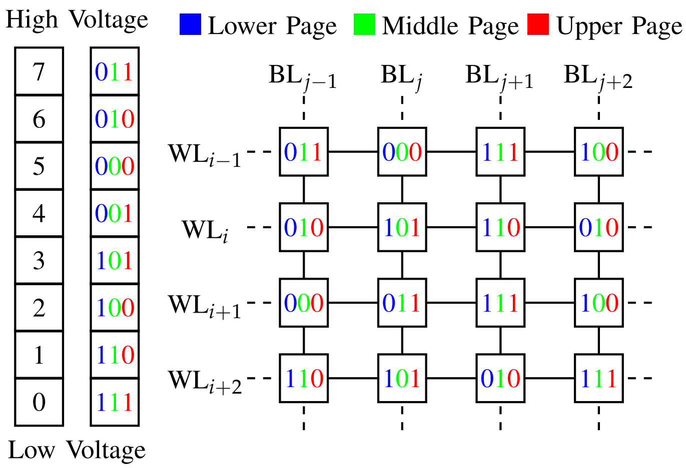


Fig. 2: (Left) Example mapping of cell program levels to binary representations in TLC. (Right) Schematic diagram of a TLC flash memory block showing the 2-D array of cells connected in the horizontal direction by wordlines (WLs) and in the vertical direction by bitlines (BLs).

generate soft read voltages from program levels over a range of program-erase cycles. When we train the networks on measured data, this conditional method can regenerate "authentic" cell-level read voltages on a 2-D array of cells from a corresponding array of program levels. We use two evaluation metrics to assess the accuracy of the results: the similarity of the histograms of read voltages, i.e., the estimated probability density functions (PDFs), and the relative frequencies of pattern-dependent ICI-induced hard read errors. As an example, Fig. 1 graphically illustrates the similarity of the estimated PDFs of data generated by a cVAE-GAN model and measured data at 4000 PE cycles. A quantitative comparison using total variation (TV) distance confirms the similarity of the distributions. More importantly, a comparison of the relative probabilities of error-inducing wordline and bitline program level patterns shows that the regenerated voltages successfully capture the spatial characteristics of the underlying 2-D ICI effects. Details of these experiments are provided in Section IV.

## II. Flash Memory Basics

### A. Block Structure and Experimental Procedure

The basic unit of data storage in NAND flash memory is a floating-gate transistor, referred to as a cell. Today's flash memories are capable of storing 1, 2, 3, 4, and 5 bits per cell representing 2, 4, 8, 16, and 32 distinct charge levels, respectively. These technologies are referred to as single-level cell (SLC), multi-level cell (MLC), triple-level cell (TLC), quad-level cell (QLC), and penta-level cell (PLC), respectively. The cells are organized into an interconnected 2-D array, called a block, via horizontal wordlines (WLs) and vertical bitlines (BLs). The flash memory chip is composed of a collection of such blocks. In 3D NAND flash devices, these 2-D arrays are stacked vertically to achieve larger volumetric density [10]. Fig. 2 depicts a schematic diagram of a planar TLC flash memory block and an example of a mapping from program levels to binary data patterns.

The basic unit of write and read operations in flash memory is a page, corresponding to a logical bit position in a wordline of a block. For TLC flash, the three pages are referred to as the lower, middle, and upper page, represented in blue, green, and red, respectively, in Fig. 2. On the other hand, the basic unit of an erase operation is an entire block.

To characterize the channel and create datasets for machine learning, we conducted program-erase (PE) cycling experiments on several blocks of a commercial 1X-nm TLC flash memory chip, as follows:

1) Erase flash memory block under test.
2) Program all pages of block under test with pseudo-random data.
3) After 4000 P/E cycles, perform a read operation on the tested block.
4) For each cell, record program level and measured voltage level.

The PE cycling experiments were performed at room temperature in a continuous manner with no wait time between the erase-program-read operations.

### B. Inter-cell Interference (ICI)

The ICI phenomenon, whereby programming of a cell induces changes in the voltage levels of neighboring cells in its block, is one of the main sources of error in flash memory. In particular, the read voltage level of a cell programmed to a low level may be inadvertently increased if its adjacent cells are programmed to high levels. For example, in TLC flash memories, if a group of three consecutive cells in a WL or BL direction are programmed with the 707 pattern, the read level of the central cell may be increased because of ICI and, during data detection, the recovered program level of the central "victim" cell may be erroneously interpreted as a level 1. To mitigate the effects of ICI, the use of constrained codes that prevent the appearance of ICI-prone patterns has been proposed; see, for example, [2], [12]. In Section IV-B, we will quantify the effect of ICI on performance in both measured data and generated data by examining the relative frequency of WL and BL patterns surrounding erroneous victim cells.

## III. Generative Modeling for Flash Memory

We adopt a conditional VAE-GAN (cVAE-GAN) architecture [6] for our generative modeling pipeline, depicted in Fig. 3. Our goal is to learn a mapping between program levels and soft read voltage levels. When sampling different latent vectors $z$ from the same distribution, we can generate multiple arrays of plausible voltages levels. The variations in these output arrays for a given array of program levels reflect the stochasticity of the channel.

### A. Generative Modeling

We first formulate generative modeling mathematically. Using the procedure outlined in Section II-A, we collect the paired channel instances in a specific PE cycle, denoted

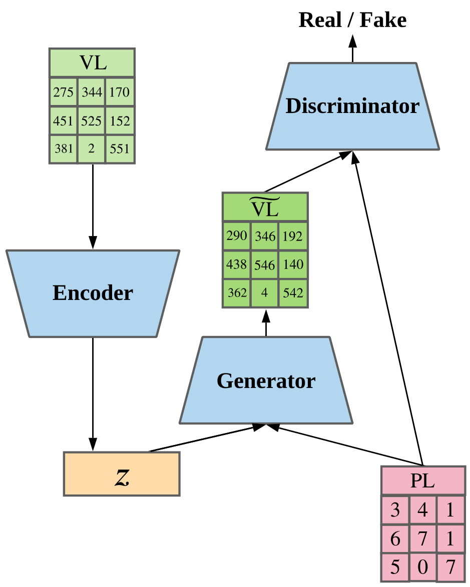


Fig. 3: Generative modeling pipeline: encoder, generator and discriminator constitute the generative modeling workflow. Here, $z$ is the latent code, PL is the array of program levels, VL is the array of measured read voltage levels, and $\widetilde{\mathrm{VL}}$ is the reconstructed array of read voltage levels. In our implementation, PL, VL, and $\widetilde{\mathrm{VL}}$ are all $64 \times 64$ arrays.

as $\{(\mathrm{PL}, \mathrm{VL}, \mathrm{PE})\}$. Program level PL is from the channel input domain $\mathcal{P}$, voltage level VL is from the channel output domain $\mathcal{V}$, and PE denotes the PE cycle. The goal of generative modeling in this paper is to learn the analytically intractable likelihood $\mathbb{P}(\mathrm{VL}|\mathrm{PL})$. This is a step toward the ultimate goal of learning the spatio-temporal nature of the data, i.e., the likelihood of VL conditioned on both PL and PE, $\mathbb{P}(\mathrm{VL}|\mathrm{PL}, \mathrm{PE})$.

There are three network modules in the workflow: encoder ($En$), generator ($Gen$), and discriminator ($Dis$). The encoder maps the read voltages to the latent code $z$ and replaces the prior distribution $\mathbb{P}(z)$ in the GAN with the learned posterior distribution $\mathbb{P}(z|\mathrm{VL})$. The decoder in the VAE shares the weights with the GAN generator. The variational lower bound [5] is given by

$$\begin{aligned}\log \mathbb{P}(\mathrm{VL}) \geq & \mathcal{L}_{KL} + \mathcal{L}_{recon} \\ = & -D_{KL}(\mathbb{Q}(z|\mathrm{VL})||\mathbb{P}(z)) + \mathbb{E}_{\mathbb{P}(z|\mathrm{VL})}[\log(\mathbb{P}(\mathrm{VL}|z))]\end{aligned}$$

where $D_{KL}$ is the Kullback-Leibler (KL) divergence. During training, the KL divergence narrows the distance between variation distribution $\mathbb{Q}(z|\mathrm{VL})$ and prior distribution $\mathbb{P}(z)$. In this work, we regard $\mathbb{P}(z)$ as a standard multivariate normal distribution and follow the re-parameterization trick [5] to sample latent vector $z$.

In the standard GAN design [1], a generator and discriminator will formulate and evaluate their fake read voltages in an adversarial game. In conditional VAE-GAN (cVAE-GAN), generator $Gen$ will take learned latent vector and PL as input and generate fake $\widetilde{\mathrm{VL}}$. The discriminator measures the difference between PL and $\widetilde{\mathrm{VL}}$. The loss in the conditional GAN part is

$$\mathcal{L}_{GAN} = \log(1 - Dis(\mathrm{PL}, Gen(\mathrm{PL}, z))) + \log(Dis(\mathrm{PL}, \mathrm{VL})).$$

Similar to VAE-GAN, we encourage the reconstructed voltage levels to match the authentic voltage levels, using the $\ell_1$-norm to measure the reconstruction loss

$$\mathcal{L}_{recon} = ||\mathrm{VL} - Gen(\mathrm{PL}, z)||_1.$$

Combining these equations, we formulate the loss function of the cVAE-GAN architecture as

$$\min_{Gen, En} \max_{Dis} \mathcal{L}_{GAN} + \alpha \mathcal{L}_{recon} + \beta \mathcal{L}_{KL}. \tag{1}$$

In Section IV, we compare the cVAE-GAN model to the conditional GAN (cGAN) [4], conditional VAE (cVAE) [14], Bicycle GAN [19], and Gaussian model. cGAN applies random noise $z$ to the generator without any variational auto-encoder module. cVAE generates the fake voltage levels without evaluations from the discriminator. Because the latent space in cVAE-GAN can only be random noise and may not utilize realistic voltage levels, Bicycle GAN incorporates a conditional latent regressor GAN into cVAE-GAN as a hybrid model. The Gaussian model derives the PDF for read voltages given a specific program level, where the mean and standard deviation are computed from measured data.

### B. Implementation Details

In TLC flash memory, each block contains hundreds of pages, each of which is typically 8-16 kB in size. In order to represent the TLC flash memory without bias, we collect data from several blocks of one 1X-nm TLC chip. We crop the blocks into non-overlapping $64 \times 64$ 2-D arrays to formulate our paired datas at 4000 PE cycles. The number of 2-D arrays in the training set is $100,000$ and the size of the evaluation dataset is $10,000$. The dimension of latent vector $z$ is set to 8.

**Remark 1.** We modify network architectures in [19] to adapt for input arrays of $64 \times 64$ program levels and $64 \times 64$ voltage levels, each of which has a single channel. The encoder network is ResNet [3], the generator network is U-net [13], and the discriminator network is PatchGAN [4].

1) Encoder: We use the two residual blocks, each of which contains two $3 \times 3$ convolutional layers with stride 1 and padding 1. We then add two linear layers, which map output features to mean and variance for the latent vector.
2) Generator: $Ck$ denotes a Convolution-BatchNorm-ReLU layer with $k$ output channels. All convolutions are $4 \times 4$ kernels applied with stride 2 and padding 1. The network architecture can be described as

$$(\text{Down Part})\ C64, C128, C256, C512, C512, C512$$

$$(\text{Up Part})\ C512, C512, C256, C128, C64, C1$$

where we inject latent vector $z$ by replication and concatenation into every layer in the "Down" part [19], and each layer in the "Up" part receives skip connections from the corresponding layer in the "Down" part [13].

3) Discriminator $Dis$: The input to the discriminator is the concatenation of fake voltage levels and program levels. With the same naming convention as in the generator, we express the discriminator as $C64, C128, C1$.

**Remark 2.** The training details of the generative modeling methods are as follows. Adam optimizer is used with learning rate $2 \times 10^{-4}$. Parameters in (1) are set to $\alpha = 10$ and $\beta = 0.01$.

1) cVAE-GAN, Bicycle-GAN, and cVAE: train for 5 epochs with batch size 2;
2) cGAN: remove latent vector in generator as in [4], train for 5 epochs with batch size 64.

During evaluation, we use program levels and latent vector $z$ sampled from a Gaussian distribution. For each program level array, we prepare 10 sampled latent vectors to evaluate the learned model.

## IV. Experimental Results

We evaluate our methods using two metrics.

1) PDF: The frequency of occurrence of each voltage level given the program level is used to estimate the conditional probability of that level. We visualize the PDFs for measured data and reconstructed data in linear and logarithmic scales. We also compare the total variation between the distributions of measured and reconstructed voltages.
2) ICI: For cells programmed to 0 that suffer an error according to the voltage level, we compute the relative frequencies of the patterns of program levels in adjacent cells in the WL and BL directions. We visualize these relative frequencies using pie charts. Numerical results are also presented for a dominant set of error patterns.

### A. PDF Analysis

As we evaluate our learned model using input arrays of program levels, we collect regenerated voltage levels and count the frequency of occurrence of voltage levels over the voltage range. We then estimate the conditional PDFs of voltages associated with each program level.

Fig. 4 shows the conditional PDFs for measured data and regenerated data in the evaluation dataset in both linear and logarithmic scales. The $x$-axis represents the soft read voltages spanning a certain voltage level range. The $y$-axis represents the conditional PDF. For program level 0, we pre-process the voltage levels due to normalization problems. From the PDF curves, we conclude that the cVAE-GAN and Bicycle GAN models produce realistic-looking distributions of voltage levels.

To detect the data, we compare voltages to thresholds determined by the intersections of adjacent conditional PDF plots in the logarithmic scale, represented by the vertical dash-dotted lines. For instance, if a voltage level lies above the first threshold but below the second threshold, the hard read level of the cell is designated as a 1.

For a quantitative comparison, we use total variation (TV) distance, $d_{TV}$, to measure the difference between the measured voltage distribution and the fake distribution. When the voltage level range is finite, $d_{TV}$ is given by

$$d_{TV}(\mathbb{P}_{real}, \mathbb{P}_{fake}) = \frac{1}{2} \sum_{\mathrm{VL}} |\mathbb{P}_{real}(\mathrm{VL}) - \mathbb{P}_{fake}(\mathrm{VL})|$$

TABLE I: Total Variation Distance of Conditional Distributions and Combined Distribution Between Measured and Generated Voltages

| PL | cVAE-GAN | Bicycle-GAN | cGAN | cVAE | Gaussian[a] |
|---|---|---|---|---|---|
| 0 | 0.7858 | 0.8399 | 0.9371 | 0.5745 | 0.9665 |
| 1 | 0.1067 | 0.0697 | 0.4210 | 0.3749 | 0.1332 |
| 2 | 0.0425 | 0.1674 | 0.0417 | 0.2449 | 0.0827 |
| 3 | 0.0737 | 0.0915 | 0.1883 | 0.2015 | 0.0832 |
| 4 | 0.0429 | 0.0575 | 0.3157 | 0.2228 | 0.0727 |
| 5 | 0.0895 | 0.0985 | 0.3315 | 0.2536 | 0.0720 |
| 6 | 0.0554 | 0.0912 | 0.1650 | 0.3001 | 0.0788 |
| 7 | 0.0311 | 0.0430 | 0.5585 | 0.3644 | 0.0793 |
| All | **0.1509** | 0.1794 | 0.3606 | 0.3162 | 0.1909 |

[a] Means and standard deviations for the Gaussian model are derived from measured data.

We compare the results obtained using the four generative modeling methods and the classical Gaussian method in Table I. The first eight rows correspond to the TV distances between the measured and regenerated conditional distributions $d_{TV}(\mathbb{P}_{real}(\mathrm{VL}|\mathrm{PL}), \mathbb{P}_{fake}(\mathrm{VL}|\mathrm{PL}))$ for the 8 program levels $\mathrm{PL} \in \{0, 1, ..., 7\}$. Among these program levels, we see that program level 0 shows the largest TV distance. The last row is the TV distance between the overall voltage distributions. According to this measure, cVAE-GAN and Bicycle-GAN are superior to the cGAN, the cVAE, and the classical Gaussian model, with cVAE-GAN achieving the smallest TV distance.

Overall, we conclude that cVAE-GAN provides the best model of the voltage levels according to visual and quantitative metrics.

### B. Characterization of ICI Effects

As discussed in Section II-B, the read voltage of a cell may be adversely increased by ICI when the neighboring cells are programmed to high levels. Cells programmed to level 0 are the most susceptible to such ICI effects. We therefore evaluate how well the models learn spatial ICI properties by examining errors associated with program level patterns $\mathrm{PL}_{i,j-1}\ \mathrm{PL}_{i,j}\ \mathrm{PL}_{i,j+1}$ and $\mathrm{PL}_{i-1,j}\ \mathrm{PL}_{i,j}\ \mathrm{PL}_{i+1,j}$ in the WL and BL directions, respectively, where the victim cell program level is 0, i.e., $\mathrm{PL}_{i,j} = 0$. When we program an interior cell to level 0, there are 64 such patterns of program levels for the pair of adjacent cells in both WL and BL directions.

We remark that classical models, such as the Gaussian model, focus on regeneration of the PDFs of the measured data and, as such, are not expected to be effective in capturing ICI effects. Also, from experiments, we find that the cVAE model produces inaccurate ICI effects.

We consider two types of pattern-dependent error probabilities. Type I error probability measures the relative frequency of occurrence of the above WL and BL patterns

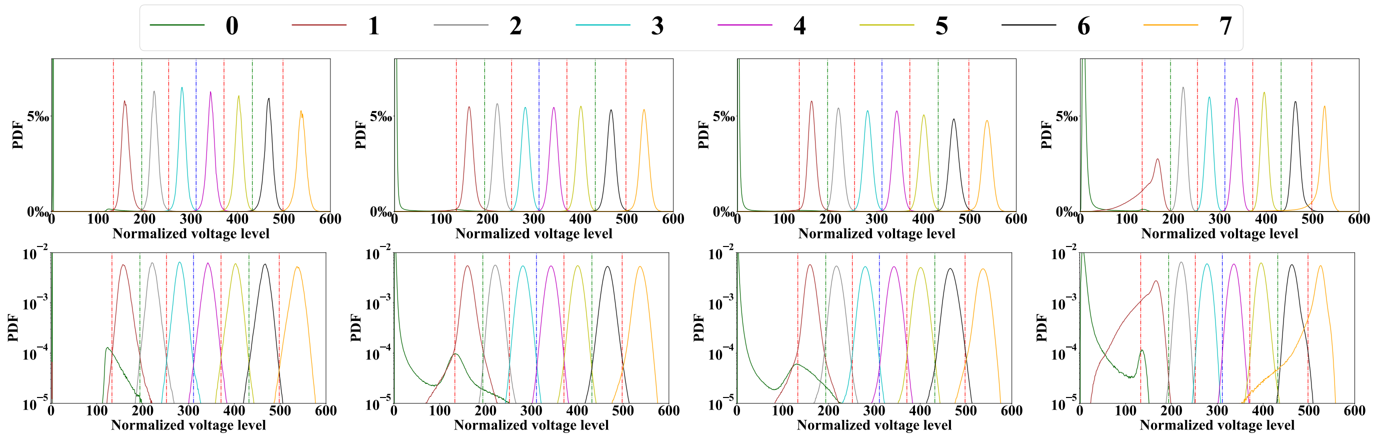


(a) Measured data (b) cVAE-GAN (c) Bicycle-GAN (d) cGAN

Fig. 4: PDF visualizations for measured, cVAE-GAN , Bicycle-GAN, and cGAN voltage levels. The first and second row of plots use a linear and logarithmic scale, respectively. Vertical dash-dotted lines are default voltage thresholds.

TABLE II: NUMERICAL VALUES OF TYPE II PATTERN-DEPENDENT ERROR RATES FOR THE 10 MOST SEVERE ICI PATTERNS

| Patterns | | 707 | 706 | 607 | 705 | 507 | 606 | 704 | 407 | 605 | 506 |
|---|---|---|---|---|---|---|---|---|---|---|---|
| Measured | Wordline | 11.60% | 7.58% | 7.73% | 5.68% | 5.78% | 5.79% | 4.53% | 4.70% | 4.32% | 4.33% |
| | Bitline | 16.17% | 11.43% | 9.24% | 9.44% | 6.58% | 5.42% | 8.48% | 5.27% | 4.19% | 3.44% |
| cVAE-GAN | Wordline | 9.16% | 7.26% | 7.07% | 5.99% | 5.99% | 5.49% | 5.17% | 5.02% | 4.26% | 4.44% |
| | Bitline | 16.37% | 12.22% | 9.59% | 9.37% | 6.35% | 5.86% | 8.06% | 4.86% | 4.29% | 3.64% |
| Bicycle-GAN | Wordline | 8.91% | 6.99% | 6.96% | 5.77% | 5.91% | 5.60% | 5.08% | 5.06% | 4.68% | 4.57% |
| | Bitline | 16.47% | 12.68% | 10.39% | 9.99% | 6.51% | 6.50% | 8.51% | 4.54% | 4.47% | 3.61% |
| cGAN | Wordline | 8.95% | 7.84% | 7.46% | 6.24% | 6.33% | 6.32% | 5.23% | 5.49% | 5.11% | 5.25% |
| | Bitline | 12.43% | 11.01% | 9.23% | 9.47% | 7.24% | 7.95% | 8.12% | 5.37% | 6.70% | 6.06% |

when an error occurs in the victim cell. More precisely, we calculate

$$\mathbb{P}(\mathrm{PL}_{i,j-1}, \mathrm{PL}_{i,j+1} | \mathrm{VL}_{i,j} > V_{th0}, \mathrm{PL}_{i,j} = 0)$$
$$\mathbb{P}(\mathrm{PL}_{i-1,j}, \mathrm{PL}_{i+1,j} | \mathrm{VL}_{i,j} > V_{th0}, \mathrm{PL}_{i,j} = 0).$$

where $V_{th0}$ denotes the voltage threshold used to distinguish between level 0 and level 1.

Type II error probability measures the probability that an error occurs in the victim cell for each of the above WL and BL patterns. Specifically, we calculate

$$\mathbb{P}(\mathrm{VL}_{i,j} > V_{th0} | \mathrm{PL}_{i,j-1}, \mathrm{PL}_{i,j} = 0, \mathrm{PL}_{i,j+1})$$
$$\mathbb{P}(\mathrm{VL}_{i,j} > V_{th0} | \mathrm{PL}_{i-1,j}, \mathrm{PL}_{i,j} = 0, \mathrm{PL}_{i+1,j})$$

Type I probabilities for measured and regenerated data are visualized in Fig. 5. In each pie chart, 23 main error patterns are explicitly presented, with the remaining patterns collectively designated by **others**. In the measured data, the 23 listed patterns account for 60% of the errors in the WL direction and around 75% of the errors in the BL direction. The dominant error pattern in both WL and BL directions is 707. For the prevalent error patterns, probabilities observed in the data generated by cVAE-GAN and Bicycle-GAN are very similar to those seen in the measured data. On the other hand, the error probabilities of the 23 main contributing patterns in cGAN are cumulatively larger, despite having a relatively smaller probability for the dominant 707 pattern. This suggests that cGAN is less successful in learning spatial ICI effects.

Table II presents the numerical values for the Type II error rates for the most error-prone patterns. In the measured data, we observe that 707 has the highest error rate in both WL and BL directions, namely 16.17% and 11.6%, respectively, and the BL error rate is about 40% larger. Overall, Type II rates in data generated by cVAE-GAN and Bicycle-GAN indicate accurate learning of ICI effects in WL and BL directions. The only substantial discrepancy is in the error rate for the 707 pattern in the WL direction, where the generated error rate, 9.16% and 8.91%, respectively, fall short of the measured error rate by about 25%.

These results show that cVAE-GAN and Bicycle-GAN both produce spatial distributions of voltage levels in a flash memory block that capture with good accuracy the effects of ICI in both vertical and horizontal directions, with the cVAE-GAN architecture giving slightly better overall results.

## V. CONCLUSION

In this paper, we explored the use of conditional generative networks to model the flash memory channel. Specifically, we trained several generative network architectures to learn spatial characteristics of read voltages in a block, conditioned on the program levels. We observe a high degree of similarity between the conditional distributions of the generated data and the measured data, both qualitatively and quantitatively. The models also capture underlying ICI effects, as measured by

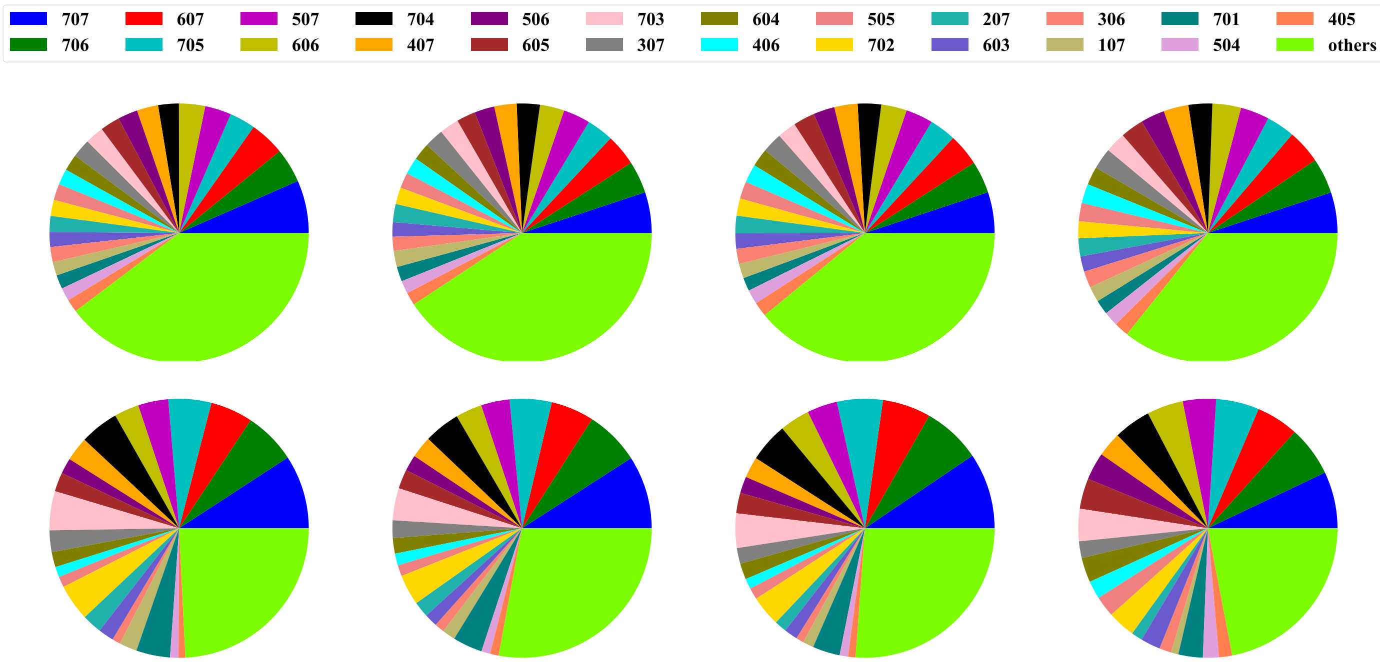


(a) Measured data (b) cVAE-GAN (c) Bicycle-GAN (d) cGAN

Fig. 5: Pie charts visualizing Type I error-causing probabilities according to measured voltages, cVAE-GAN generated voltages, Bicycle-GAN generated voltages, and cGAN generated voltages. The sector labeled **others** combines 41 lesser frequency patterns. The first row of pie charts correspond to the WL direction and the second row to the BL direction.

two types of pattern-dependent error probabilities. Taking all of these metrics into account, we conclude that the cVAE-GAN offers a realistic model of flash memory read voltages. These results motivate further investigation into generative modeling architectures for flash memory channels that can better learn spatial characteristics, and also learn temporal characteristics due to cycling and retention.

## ACKNOWLEDGMENT

The authors would like to thank Zachary Blair and Yi Liu for establishing the flash memory test platform used in this study. The authors would also like to acknowledge very helpful discussions with Naoaki Kokubun.

## REFERENCES

[1] I. J. Goodfellow, J. P.-Abadie, M. Mirza, B. Xu, D. W.-Farley, S. Ozair, A. Courville, and Y. Bengio, "Generative adversarial nets," in *Proc. Neural Inf. Process. Syst. (NIPS)*, Montréal, Canada, Dec. 2014, pp. 2672–2680.

[2] A. Hareedy and R. Calderbank, "LOCO codes: Lexicographically-ordered constrained codes," *IEEE Trans. Inf. Theory*, vol. 66, no. 6, pp. 3572–3589, June 2020.

[3] K. He, X. Zhang, S. Ren, and J. Sun, "Deep residual learning for image recognition," in *Proc. IEEE Conf. Comput. Vis. Pattern Recognit. (CVPR)*, Las Vegas, NV, USA, July 2016, pp. 770–778.

[4] P. Isola, J-Y. Zhu, T. Zhou, A. A. Efros, "Image-to-image translation with conditional adversarial networks," in *Proc. IEEE Conf. Comput. Vis. Pattern Recognit. (CVPR)*, Honolulu, HI, USA, July 2017, pp. 1125–1134.

[5] D. P. Kingma and M. Welling, "Auto-encoding variational bayes," in *Proc. Int. Conf. Represent. Learn. (ICLR)*, Banff, Canada, Apr. 2014.

[6] A. B. L. Larsen, S. K. Sønderby, H. Larochelle, O. Winther, "Autoencoding beyond pixels using a learned similarity metric," in *Int. Conf. Mach. Learn. (ICML)*, New York, USA, June 2016.

[7] Y. Liu, S. Wu, and P. H. Siegel, "Bad Page Detector for NAND Flash Memory," in *Annual Non-Volatile Memories Workshop (NVMW)*, CA, USA, Mar. 2020.

[8] Z. Liu, Y. Liu, and P. H. Siegel, "Generative modeling of NAND flash memory voltage level," in *Non-Volatile Memories Workshop (NVMW)*, CA, USA, Mar. 2021.

[9] Y. Luo, S. Ghose, Y. Cai, E. F. Haratsch and O. Mutlu, "Enabling accurate and practical online flash channel modeling for modern MLC NAND flash memory," *IEEE J. Select. Areas Commun.*, vol. 34, no. 9, pp. 2294-2311, Sept. 2016.

[10] N. Papandreou, H. Pozadis, T. Parnell, N. Loannoum, R. Pletka, S. Tomic, P. Breen, G. Tressler, A. Fry, and T. Fisher, "Characterization and analysis of bit errors in 3D TLC NAND flash memory," in *IEEE Int. Relilability Phys. Symp. (IRPS)*, Monterey, CA, USA, Apr. 2019.

[11] T. Parnell, N. Papandreou, T. Mittelholzer, and H. Pozidis,"Modelling of the threshold voltage distributions of sub-20nm NAND flash memory," in *Proc. IEEE Global Commun. Conf.*, Dec. 2014, pp. 2351–2356.

[12] M. Qin, E. Yaakobi, and P. H. Siegel, "Constrained codes that mitigate inter-cell interference in read/write cycles for flash memories," *IEEE J. Select. Areas Commun.*, vol.32, no.5, pp. 836–846, May 2014.

[13] O. Ronneberger, P. Fischer, and T. Brox, "U-Net: convolutional networks for biomedical image segmentation," in *Int. Conf. Med. Imag. Comput. Comput.-assisted Intervention (MICCAI 2015)*, Springer, Cham.

[14] K. Sohn, H. Lee, and X. Yan "Learning structured output representation using deep conditional generative models," in *Proc. Neural Inf. Process. Syst. (NIPS)*, Montréal, Canada, Dec. 2015.

[15] N. Sree Prem, "An Application of Machine Learning to Bad Page Prediction in Multilevel Flash," Master's Thesis, University of California San Diego, 2019.

[16] V. Taranalli, H. Uchikawa, and P. H. Siegel, "Channel models for multi-level cell flash memories based on empirical error analysis," *IEEE Trans. Commun.*, vol. 64, no. 8, pp. 3169–3181, Aug. 2016.

[17] V. Taranalli, H. Uchikawa, and P. H. Siegel, "Error analysis and inter-cell interference mitigation in multi-level cell flash memories," in *Proc. IEEE Int. Conf. Commun. (ICC)*, London, U.K., June 2015, pp. 271–276.

[18] S. Zheng, Y. Liu, and P. H. Siegel, "PR-NN: RNN-based detection for coded partial-response channels," *IEEE J. Select. Areas Commun.*, vol. 39, no. 7, pp. 1967–1982, July 2021.

[19] J-Y. Zhu, R. Zhang, D. Pathak, T. Darrell, A. A. Efros, O. Wang, and E. Shechtman, "Toward multimodal image-to-image translation," in *Proc. Neural Inf. Process. Syst. (NIPS)*, Montréal, Canada, Dec. 2017, pp. 465–476.